Title

Hyperpolarized 13C magnetic resonance evaluation of renal ischemia reperfusion injury in a murine model

Journal

NMR in Biomedicine, 30(10)

ISSN

0952-3480

Authors

Baligand, Celine
Qin, Hecong
True-Yasaki, Aisha
et al.

Publication Date

2017-10-01

DOI

10.1002/nbm.3765

Peer reviewed

HHS Public Access

Author manuscript

NMR Biomed. Author manuscript; available in PMC 2018 October 01.

Published in final edited form as:

NMR Biomed. 2017 October ; 30(10): . doi:10.1002/nbm.3765.

Hyperpolarized ^{13}C Magnetic Resonance Evaluation of Renal Ischemia Reperfusion Injury in a Murine Model

Celine Baligand[*,1], **Hecong Qin**[*,1], **Aisha True-Yasaki**[1], **Jeremy Gordon**[1], **Cornelius von Morze**[1], **Justin DeLos Santos**[1], **David Wilson**[1], **Robert Raffai**[2], **Patrick M. Cowley**[2], **Anthony J. Baker**[2], **John Kurhanewicz**[1], **David H. Lovett**[2], and **Zhen Jane Wang**[1]

[1]Radiology and Biomedical Imaging, University of California San Francisco, San Francisco, CA

[2]Medicine, San Francisco VAMC/University of California San Francisco, San Francisco, CA

Abstract

Acute kidney injury (AKI) is a major risk factor for the development of chronic kidney disease (CKD). Persistent oxidative stress and mitochondrial dysfunction are implicated across diverse forms of AKI and in the transition to CKD. In this study, we applied hyperpolarized (HP) ^{13}C dehydroascorbate (DHA) and ^{13}C pyruvate MR spectroscopy to investigate the renal redox capacity and mitochondrial pyruvate dehydrogenase (PDH) activity, respectively, in a murine model of AKI at baseline, and 7 days after unilateral ischemia reperfusion injury (IRI). Compared to the contralateral sham-operated kidneys, the kidneys subjected to IRI showed a significant decrease in the HP ^{13}C Vitamin C/(Vitamin C+DHA) ratio, consistent with a decrease in redox capacity. The kidneys subjected to IRI also showed a significant decrease in the HP ^{13}C bicarbonate/pyruvate ratio, consistent with impaired PDH activity. The IRI kidneys showed a significantly higher HP ^{13}C lactate/pyruvate ratio at day 7 compared to baseline, although the ^{13}C lactate/pyruvate ratio was not significantly different between the IRI and the contralateral sham-operated kidneys at day 7. Arterial spin labeling MRI demonstrated significantly reduced perfusion in the IRI kidneys. Renal tissue analysis showed corresponding increased reactive oxygen species (ROS), and reduced PDH activity in the IRI kidneys. Our results show the feasibility of HP ^{13}C MR for the noninvasive assessment of oxidative stress and mitochondrial PDH activity following renal ischemia reperfusion injury.

Graphical abstract

We have shown that hyperpolarized ^{13}C dehydroascorbate and ^{13}C pyruvate MRS can be used to noninvasively assess the altered renal redox capacity and mitochondrial PDH activity following ischemia reperfusion injury in a murine model. Such an imaging approach can potentially enhance the prediction and monitoring of progressive kidney injury.

Correspondence and Reprint Request: Zhen Jane Wang, MD, Department of Radiology and Biomedical Imaging, University of California, San Francisco, San Francisco, CA 94143, Tel: (415) 476-3767, Fax: (415) 514-0414, jane.wang@ucsf.edu.

*These authors contributed equally.

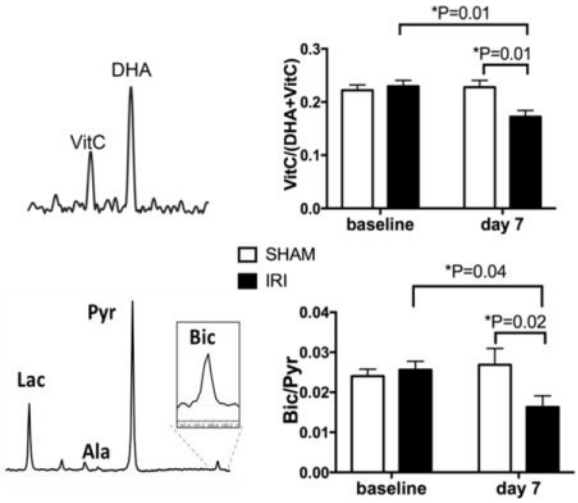

Introduction

Acute kidney injury (AKI) occurs frequently in hospitalized patients. A leading cause of AKI is renal ischemia reperfusion injury (IRI) that occurs in patients with cardiovascular disease, sepsis, following surgery, or in the context of a kidney transplant. Although the kidneys have a remarkable reparative capacity, the repair of AKI is often incomplete with maladaptive responses that contribute to the transition to chronic kidney disease (CKD). Indeed, AKI has been shown to be a major risk factor for the subsequent development of CKD [1–4], which is increasing in incidence and represents a major public health concern in the United States [5].

Persistent oxidative stress and mitochondrial dysfunction are strongly implicated across diverse forms of AKI and in the transition to CKD [6–12]. For example, both AKI and CKD are characterized by an over-production of oxidants in the presence of a diminished antioxidant reserve. This alteration in redox regulation has been shown to promote renal fibrosis and CKD [7]. Additionally, the altered redox regulation leads to mitochondrial dysfunction that further exacerbates kidney injury. Recent evidence has shown that renal tubules undergoing atrophy late after IRI displayed decreased mitochondrial pyruvate dehydrogenase (PDH) activity and oxidative phosphorylation, and increased glycolysis [12]. The recognition of these cellular and molecular events, and metabolic alterations following AKI has also motivated research into mechanistically-targeted therapies to treat AKI and to prevent progression to CKD [13, 14]. Therefore, biomarkers that can noninvasively inform on renal oxidative stress and mitochondrial dysfunction have the potential to improve the CKD risk stratification of patients following AKI, and aid in the determination of efficacy of targeted therapies.

The development of hyperpolarized (HP) ^{13}C MR spectroscopy and imaging based on dissolution dynamic nuclear polarization (DNP) has enabled unprecedented noninvasive visualization of normal and abnormal metabolism in living systems [15–17]. HP ^{13}C dehydroascorbate (DHA) has been shown to permit *in vivo* assessment of localized redox capacity [18, 19]. DHA is an oxidized form of Vitamin C (VitC), and is reduced to VitC via

a glutathione-dependent mechanism, with coupled reactions to NADPH. Prior studies in several preclinical disease models have shown that the rate of HP ^{13}C DHA reduction to ^{13}C VitC is related to the levels of reduced glutathione (GSH), and to the rate of NADPH production from the pentose phosphate pathway [18–20]. As GSH and NADPH are key antioxidants that counteract reactive oxygen species (ROS), HP ^{13}C DHA reduction to ^{13}C VitC should reflect tissue redox capacity and may serve as an indicator for cellular oxidative stress. Pyruvate, a critical substrate for energy metabolism, is metabolized to downstream products including lactate and alanine in the cytosol, and it is also shuttled into the mitochondria and converted to acetyl-CoA via the enzyme pyruvate dehydrogenase (PDH) in the first step of oxidative phosphorylation. The byproduct of this first step, CO_2, rapidly equilibrates with bicarbonate. Accordingly, monitoring the production of HP ^{13}C bicarbonate from [1-^{13}C] pyruvate should enable the assessment of PDH activity *in vivo* [21, 22].

In this study, we applied HP [1-^{13}C] DHA and [1-^{13}C] pyruvate MR to investigate the renal redox capacity and mitochondrial PDH activity, respectively, in a murine model of AKI induced by ischemia reperfusion.

Methods

Experimental design

All procedures in this study were performed in accordance with the Principles for the Utilization and Care of Vertebrate Animals, and were approved by the Institutional Animal Care & Use Committee.

MR studies were performed in a group (n=15) of male FVB mice (Charles River Laboratory, USA) 3 to 5 months of age at baseline, and 7 days following unilateral ischemia reperfusion injury (IRI). The unilateral IRI model was created by temporarily occluding the left renal pedicle and a sham operation on the contralateral kidney without occluding the renal pedicle, as described in detail in the below section. In a subgroup of the mice (n=6), kidneys were harvested for histological and enzyme (pyruvate dehydrogenase (PDH) and lactate dehydrogenase (LDH)) analyses after the day 7 MR studies. In addition, blood samples were collected at baseline and day 7 for quantification of blood urea nitrogen.

Previous studies in similar mouse models of unilateral renal IRI have reported that day 7 is representative of a time point at which the kidneys transition from acute tubular necrosis to attempted repair [12, 23]. To confirm this finding in our study, renal sections from a separate group of FVB mice 48 hours following unilateral IRI were assessed for tubular injury, and compared to those 7 days following unilateral IRI and to control mice not subjected to IRI.

An additional group of FVB mice (n=5) were subjected to sham operation without unilateral IRI. The kidneys were harvested at day 7, and renal LDH activity was compared to that of kidneys from the unilateral IRI model. This was performed to assess the potential effect of sham operation on LDH activity. This group of mice did not undergo MR studies.

Ischemia reperfusion protocol

Animals were anaesthetized with inhaled isoflurane (2% isoflurane mixed in O_2 delivered at 1 L/min). The back of the animal was shaved and cleaned, and an incision was made to localize the left kidney. After the left renal pedicle was isolated from surrounding structures, unilateral renal ischemia was induced by clamping the renal pedicle with an atraumatic vascular clamp for 40 minutes. After ischemia, the clamp was removed to allow for reperfusion, and kidney was visually monitored until a pink color was restored. The incision was closed in 2 layers with a 5-0 chromic suture. During the 40 min ischemia period, a sham operation was performed on the contralateral kidney. A similar incision was done, and the right kidney and renal pedicle were exposed but the vessels were not clamped.

Hyperpolarized ^{13}C DHA MR

HP [1-^{13}C] DHA injection combined with 3D ^{13}C MR spectroscopic imaging were used to interrogate kidney redox capacity as previously published [18, 24]. The mice were fasted for 8 hours during the day prior to the MR studies, and the MR studies were performed at about the same time during the day to minimize any physiological variations. Mice were fasted before the MR studies to minimize any potential variability related to food intake because DHA is taken up by cells via the glucose transporters Glut1, 3, and 4 [25]. Under anaesthesia (2% isoflurane in 1 L/min oxygen), a tail vein catheter was placed for intravascular access and animals were placed supine in a dual-tuned ^{1}H–^{13}C quadrature RF coil. Experiments were conducted using a 3T MRI scanner (GE Healthcare, USA) equipped with MNS (multinuclear spectroscopy) hardware package. The HP ^{13}C DHA study was performed at 3T to take advantage of the significantly longer T_1 relaxation time of HP ^{13}C DHA and VitC at lower field (3T: T1=56.5s and 29.2s for DHA and VitC, respectively. 11.7T: T1=20.5s and 16s for DHA and VitC, respectively) [24]. Coronal and sagittal T2-weighted images were acquired for anatomic localization using a standard fast spin echo (FSE) sequence (TE/TR=100ms/6112ms for sagittal acquisition, TE/TR=100ms/4657ms for coronal acquisition, slice thickness=1.5mm, FOV=80mm×40mm, matrix=256×256, number of average =6). A 2.2M solution of [1-^{13}C] DHA in dimethyacetamide (DMA) containing 15mM OX063 trityl radical (GE Healthcare) was polarized on a HyperSense DNP instrument (Oxford Instruments, UK) operating at 3.35T and 1.3° K. The frozen sample was dissolved in distilled water containing 0.3 mM ethylenediaminetetracetic acid (EDTA). The average polarization level for the HP [1-^{13}C] DHA was approximately 10.1%. HP [1-^{13}C] DHA (250 μL, 21mM, approximate pH of 5) was injected over 15s through a tail vein catheter. 3D ^{13}C echo planar spectroscopic imaging (EPSI) was acquired 25 seconds after the start of the injection: single spin- echo, ramp-sampled, symmetric EPSI readout, and concentric ring k-space sampling. This pulse sequence was similar to a previously described one used for rapid HP ^{13}C spectroscopic imaging [26]. In our study, however, a single adiabatic spin-echo rather than a double adiabatic spin-echo pulse sequence was used because only a single time point was acquired, reducing the TE and improving SNR. The other acquisition parameters were as follows: FOV=48mm × 48mm × 96mm, matrix size=8×8×16 (zero filling in z direction), resolution= 6×6×6 mm^3, spectral bandwidth=540Hz, TR=185ms, TE=115ms, variable flip angle scheme with final flip angle 90°, total scan time=12 seconds. The MR data were processed using an open-source

software package “Spectroscopic Imaging Visualization and Computing” (SIVIC) [27], and data were expressed as peak magnitude height VitC/(VitC+DHA) ratio.

Hyperpolarized ^{13}C pyruvate MR

HP ^{13}C pyruvate MR experiments were conducted on a 14.1 T vertical system (Agilent Technologies, USA) using a dual-tuned ^{13}C-^{1}H birdcage coil (M2M imaging Corporation, USA), within one day of the HP ^{13}C DHA MR experiments. The mice were not fasted before the ^{13}C pyruvate MR studies, as fasting has been shown to reduce ^{13}C bicarbonate signal in the kidneys [28]. The MR studies were performed at about the same time during the day to minimize any physiologic variations. A mixture of [1-^{13}C] pyruvate (Sigma), 15mM trityl radical (GE Healthcare), and 1.5 mM Gd-DOTA (Guerbet, France) was polarized using a HyperSense DNP instrument. The polarized compound was rapidly dissolved in 4.5mL of a pH-balanced heated buffer solution, and 350 μL of the resulting solution (160mM, approximate pH of 7) were injected into the mouse through a tail vein catheter over 10s. The average polarization level for the HP [1-^{13}C] pyruvate was approximately 23.4%. 2D ^{13}C chemical shift imaging was acquired 25s after the start of the injection using the following parameters: RF bandwidth =10000Hz, FOV=32 × 32 mm^2, slab thickness=8mm, matrix=8×8, resolution=4mmx 4mm × 8mm, TR=66ms, TE=0.45ms, spectral bandwidth 4223Hz, constant flip angle 10°, number of excitation=64, total acquisition time 4.2s. Data were post-processed in MestReNova (Mestrelab Research S. L., Spain). Spectra were corrected for phase and baseline, and peak integration was performed for pyruvate (Pyr), lactate (Lac), alanine (Ala), and bicarbonate (Bic). Results were presented as ratios of these metabolite signal integrations (Lac/Pyr, Ala/Pyr, Bic/Pyr, Bic/Lac).

Renal perfusion by arterial spin labeling (ASL) ^{1}H-MRI

Immediately after the HP ^{13}C pyruvate MR studies, renal perfusion was measured at 14.1T using a pre-saturated pulsed ASL-FSE sequence with fat suppression and respiratory triggering as described previously [29, 30]. The slice of interest was off-centered by 9mm in order for the sensitive region of the coil to cover the heart and to allow efficient blood labelling. The acquisition parameters were as follows: 1) Five slice-selective (4mm thickness) pre-saturation pulses (sinc5, 2ms, randomized crusher gradients); 2) Non-selective or slice-selective inversion (1.1 mm thickness, 180° hyper secant adiabatic full passage pulse, 3.5 ms); 3) inversion time TI=1.5ms; 4) fat suppression pulse (sinc, 6 ms); 5) FSE imaging (500μ gauss pulse, echo-train length= 32, inter echo time=2.8ms, matrix size=128×128, FOV=30×30mm^2, slice thickness= 2mm, 30 averages, overall TR= 6s). The respiration of the mice was kept at a rate ranging between 80 and 100 breath per minute to ensure that the tagging module and the imaging module occurred during the quiescent phase of the respiratory cycle [29]. Perfusion maps were generated in MATLAB (Mathworks Inc) as previously described [29], and expressed in ml/min/100g of tissue.

Kidney volume measurement

High resolution respiratory triggered T2 weighted spin echo axial images were acquired for kidney volume calculation using the following parameters: TE, 20ms; TR,1200ms; FOV, 32mm; matrix, 16×16; number of signal average, 2; number of slices: 16; slice thickness:

1mm, no gap. The kidney volume was calculated by first multiplying the cross section area of each kidney slice by the slice thickness and then summing the values of all the kidney slices as previously described [31].

Blood urea nitrogen assay

Serum blood urea nitrogen (BUN) of the mice at baseline and 7 days following unilateral IRI was measured using a commercially available assay kit (Arbor Assays, USA) and according to the manufacturer's instructions. The sample was measured spectrophotometrically at 450 nm at room temperature using an Infinite M200 microplate reader (Tecan Group Ltd., Switzerland), and the results were expressed in mg/dl urea nitrogen.

Renal histology

After the kidneys were rapidly dissected and harvested from the mice, one half of the kidney was immediately formalin-fixed for renal histology analysis, the other half was snap frozen in liquid nitrogen and stored at −80° C for subsequent dichlorohydrofluorescein (DCF) stain and enzyme activity analysis described below. For renal histology, 5 μm thick renal sections were cut from 10% formalin-fixed, paraffin-embedded kidney samples, and stained with periodic acid-Schiff (PAS). Six randomly chosen fields at 200× magnification were examined, and scored on a 0–4 injury scale as previously described [32]: 0=normal, 1=loss of brush border and/or tubule debris, 2=loss of nuclei, 3=partial tubule obstruction, and 4=tubule obstruction and dilatation.

Reactive oxygen species (ROS) detection using dichlorohydrofluorescein (DCF) stain

Renal frozen sections (8 μm) were incubated for 30 min at 37 ° C with the fluorescent dye, 2′–7′-DCF-diacetate (20 μM, Invitrogen/Molecular Probes). Sections were rinsed and incubated for an additional 15 minutes at 37 ° C. Following rinsing, the sections were mounted in anti-fade/DAPI medium (Invitrogen) and examined by confocal microscopy.

Pyruvate dehydrogenase (PDH) and lactate dehydrogenase (LDH) activity assay

In vitro PDH activity was measured by coupling to the reduction of NAD^+ (nicotinamide adenine dinucleotide) to NADH, using a commercially available kit (Abcam, USA). NADH concentration was measured spectrophotometrically at 450 nm at room temperature using an Infinite M200 microplate reader, and the results were expressed as change of absorbance per minute per mg of protein.

In vitro LDH activity was measured spectrophotometrically by quantifying the linear decrease in NADH absorbance at varying pyruvate (sodium salt) concentrations at 339 nm using an Infinite M200 microplate reader. The maximum velocity (Vmax) and the Michaelis-Menten constant (Km) were estimated using the Lineweaver-Burk plot.

Statistical analysis

Data were presented as mean± standard error of the mean (SEM). A Levene's test was performed first to examine the homogeneity of variance of the MR data. For those data that demonstrate homogeneity of variance (VitC/(VitC+DHA), Bic/Pyr, Bic/Lac), a standard

two-way analysis of variance (ANOVA) was used to examine the main and interactive effects of time (baseline versus day 7) and kidney (sham operated kidney versus IRI kidney). Then, a paired student t-test was used to compare the metabolite ratios between baseline and day 7 in the IRI and contralateral sham-operated kidneys, and to compare the metabolite ratios between the IRI and the contralateral sham-operated kidneys at day 7. The Benjamini-Hochberg procedure was used to adjust for multiple comparisons. For the metabolite ratios that do not demonstrate homogeneity of variance (Lac/Pyr, Ala/Pyr), a standard two-way ANOVA was not used, and paired t-tests adjusted for multiple comparisons were used directly to compare the metabolite ratios between baseline and day 7 in the IRI and contralateral sham-operated kidneys, and to compare the metabolite ratios between the IRI and the contralateral sham-operated kidneys at day 7. A paired student t-test was also used to compare the renal tissue PDH and LDH activity between the IRI and contralateral sham-operated kidneys at day 7, as well as the blood urea nitrogen level pre and post IRI. Data were tested and confirmed to be normally distributed using the Shapiro Wilk test prior to student t-test analysis. The Wilcoxon signed-rank test was used to compare the injury scores in the IRI and contralateral sham-operated kidneys at day 7. In all tests, a two tailed $p<0.05$ was considered statistically significant.

Results

Table 1 shows the animal weight, BUN, and kidney volumes measured by MRI at baseline and 7 days following unilateral IRI. The BUN level was significantly higher following IRI, indicating renal dysfunction. While the volume of the kidney subjected to IRI remained the same at day 7 when compared to baseline, the contralateral sham-operated kidney volume increased at day 7 ($p<0.0005$), consistent with compensatory hypertrophy.

Hyperpolarized ^{13}C DHA MR

Fig. 1A shows representative HP ^{13}C DHA spectra through the kidneys. Fig. 1B shows the ratio of VitC/(VitC+DHA) for the kidneys at baseline and day 7. A two-way ANOVA showed that the changes of VitC/(VitC+DHA) ratio over time were significantly different for the sham-operated and IRI kidneys (N=15) ($p=0.008$). The IRI kidneys showed significantly lower VitC/(VitC+DHA) ratio at day 7, consistent with lower redox capacity (IRI kidneys: 0.23 ± 0.01 at baseline, 0.17 ± 0.01 at day 7; contralateral sham-operated kidneys: 0.22 ± 0.01 at baseline, 0.23 ± 0.01 at day 7; $p=0.01$ when comparing baseline to day 7 for the IRI kidney; $p=0.01$ when comparing the IRI and contralateral sham-operated kidneys at day 7).

Hyperpolarized ^{13}C pyruvate MR

Fig. 2A and 2B show representative spectrum from a kidney voxel in the IRI kidney at day 7, and HP ^{13}C metabolites lactate (Lac), alanine (Ala) and bicarbonate (Bic) after injection of HP ^{13}C pyruvate. Fig. 2C–E show the HP ^{13}C Bic/Pyr, Lac/Pyr, and Ala/Pyr ratios for the kidneys at baseline and day 7 following unilateral IRI. A two-way ANOVA showed that the changes of Bic/Pyr ratio over time were significantly different for the sham-operated and IRI kidneys (N=15) ($p=0.03$). The ^{13}C Bic/Pyr ratio in the IRI kidneys decreased significantly from baseline (0.026 ± 0.002) to day 7 (0.016 ± 0.003) ($p=0.04$), and the Bic/Pyr ratio was

significantly lower in the IRI than the contralateral sham-operated kidneys at day 7 (IRI: 0.016 ± 0.003; sham: 0.027± 0.004; p=0.02). The ^{13}C Lac/Pyr ratio increased significantly from baseline (0.267± 0.026) to day 7 (0.381± 0.043) in the IRI kidneys (p=0.04). However, the ^{13}C Lac/Pyr ratio was not significantly different between the sham-operated and IRI kidneys at day 7 (p=0.35). The ^{13}C Ala/Pyr ratio remained the same following IRI (p=0.33). We also evaluated the ratio of ^{13}C Bic/Lac as another measure of oxidative pyruvate metabolism that is independent of the ^{13}C pyruvate delivery (Fig. 4F). The two-way ANOVA showed that the changes of Bic/Lac ratio over time were significantly different for the sham-operated and IRI kidneys (N=15) (p=0.03). The ^{13}C Bic/Lac ratio in the IRI kidneys decreased significantly from baseline to day 7 (baseline: 0.102± 0.008; day 7: 0.051± 0.008; p=0.001). The ^{13}C Bic/Lac ratio in the sham-operated kidneys decreased slightly from baseline to day 7 (baseline: 0.097± 0.006; day 7: 0.082± 0.007; p=0.045). The ^{13}C Bic/Lac ratio was significantly lower in the IRI than the sham-operated kidneys at day 7 (IRI: 0.051± 0.008; sham-operated: 0.082± 0.007; p=0.02).

^{1}H ASL MRI

Fig. 3A shows an example of a renal perfusion map as measured by ASL MRI. Seven days after unilateral IRI, perfusion was significantly decreased in the injured kidneys, from 516 ± 22 mL/min/100g at baseline to 243 ± 15 mL/min/100g on day 7 (p<0.001), and remained virtually unchanged in the contralateral sham-operated kidney (Fig. 3B).

Renal histology

Representative results of PAS-stained renal sections are shown in Fig. 4. Control kidneys from mice not subjected to unilateral IRI showed normal tubular structures (Fig. 4A). Kidneys at 48 hours after being subjected to unilateral IRI showed moderate injury with tubular dilatation and cast formation (Fig. 4B). Kidneys at 7 days after being subjected to unilateral IRI showed diminished cast formation and tubular dilatation associated with regenerating tubular epithelial cells (Fig. 4C). The contralateral sham-operated kidneys at day 7 showed scattered foci of tubular epithelial cell necrosis associated with cellular cast formation (Fig. 4D). At day 7, the kidneys subjected to unilateral IRI had significantly higher injury scores compared to the contralateral sham-operated kidneys (2.4±0.8 vs. 0.5±0.5, p<0.001).

Dichlorohydrofluorescein stain

Representative results of DCF staining of the renal sections are shown in Fig. 5. The kidneys subjected to unilateral IRI showed markedly higher DCF staining, consistent with increased ROS, compared to the contralateral sham-operated kidneys at day 7.

PDH and LDH activity

At day 7, the PDH activity of the IRI kidneys was significantly lower than that of the contralateral sham-operated kidneys (IRI: 30.5±29.6 ΔmOD450/min/mg protein, sham-operated: 154.7±32.2 ΔmOD450/min/mg protein, p=0.005).

At day 7, there was no significant difference in the LDH activity (Vmax) between the IRI kidneys and the contralateral sham-operated kidneys (IRI: 0.52±0.04 μM NADH/min/mg

protein, sham-operated: 0.48±0.02 μM NADH/min/mg protein, p= 0.29). For the separate group of mice that underwent sham surgery without unilateral IRI, at day 7, the kidney LDH activity (Vmax) was 0.34±0.03 μM NADH/min/mg protein, significantly lower than that of the IRI kidneys or the contralateral sham-operated kidneys in the unilateral IRI model (p=0.02, and p=0.01 respectively).

Discussion

AKI is a leading cause of morbidity and mortality in hospitalized patients, and a major risk factor for the subsequent development of CKD. Prior studies have suggested that oxidative stress and mitochondrial dysfunction are key events that promote the transition from AKI to CKD [6–12]. In a murine model of unilateral IRI, we have shown that HP ^{13}C MR can be used to noninvasively monitor the altered redox capacity and mitochondrial PDH activity following AKI.

In this study, we evaluated the metabolic changes in the kidneys at day 7 following unilateral IRI. Previous studies in similar mouse models of unilateral IRI have shown that this time point is representative of a stage during which the kidneys transition from acute tubular necrosis to attempted repair where the surviving renal tubular epithelial cells regenerate [12, 23]. In agreement, our histological assessment of the renal sections at day 7 following unilateral IRI demonstrated diminished tubular injury associated with tubular epithelial cell regeneration. However, such repair has been shown to be frequently incomplete and dysfunctional, with some renal tubular cells undergoing premature growth arrest with subsequent tubular atrophy [12]. Investigation of the metabolic changes at this stage represents an important step in better understanding the events that may promote the transition from AKI to CKD.

We found an approximately 25% lower HP ^{13}C VitC/(VitC+DHA) ratio in the kidneys 7 days following unilateral IRI. We have previously reported in a murine model of diabetic nephropathy (db/db mice) that renal HP ^{13}C DHA reduction to Vitamin C (VitC) reflects glutathione (GSH) concentration [18]. GSH protects cells from oxidative stress by preventing the accumulation of ROS. GSH is a cofactor of dehydroascorbate reductase, which recycles DHA back to reduced ascorbic acid (Vitamin C), therefore linking the redox couple between glutathione and Vitamin C. A recent study in a tumor model also showed that the rate of HP ^{13}C DHA reduction to VitC depends both on GSH level as well as the rate of NADPH production from the pentose phosphate pathway, and reflects the capacity of tumor to resist oxidative stress [20]. It should also be noted that DHA reduction can be affected by redox enzymes such as glutaredoxin and glutathione-S-transferase omega that have DHA reductase activity [33, 34]. Therefore the rate of DHA reduction to VitC can be affected by multiple components of the complex redox machinery. Nonetheless, our observed lower DHA reduction to VitC in the kidneys subjected to IRI, reflected by the lower VitC/(VitC+DHA) ratio, is consistent with reduced redox capacity and higher oxidative stress in the IRI kidneys. Correspondingly, the renal sections from the kidneys subjected to IRI showed marked dichlorohydrofluorescein (DCF) staining consistent with higher ROS, when compared to those from the contralateral sham-operated kidneys.

We found a mean decrease of 36% in the HP ^{13}C Bic/Pyr ratio from baseline to day 7 in the kidneys subjected to IRI. In the kidneys, multiple tubular transport processes require high level of ATP generation, which is derived almost exclusively from mitochondrial oxidative phosphorylation [35]. In renal tubular cells, pyruvate is taken up by the mitochondria for oxidative phosphorylation and ATP production. In the first step of oxidative phosphorylation, the mitochondrial enzyme PDH irreversibly converts pyruvate into acetyl-CoA, and CO_2 which is in equilibrium with bicarbonate (Bic). Thus the HP ^{13}C Bic/Pyr ratio reflects a net flux via PDH. Corresponding to the lower HP ^{13}C Bic/Pyr ratio, we also found significantly reduced PDH activity in the homogenate of the kidneys subjected to IRI when compared to the contralateral sham-operated kidneys.

We found that the HP ^{13}C Lac/Pyr ratio increased by approximately 42% from baseline to day 7 in the kidneys subjected to IRI. This may be related to a shift towards glycolysis as a result of the mitochondrial dysfunction and reduced oxidative phosphorylation. Interestingly, although the ^{13}C Lac/Pyr ratio increased significantly from baseline to day 7 in the IRI kidneys, the ^{13}C Lac/Pyr ratio was not significantly different between the IRI kidneys and contralateral sham-operated kidneys at day 7. This appears to be related to an increase in the Lac/Pyr ratio in the sham-operated kidneys as well from baseline to day 7, although the increase in the sham-operated kidneys was not statistically significant. A prior study has shown that unilateral renal IRI causes release of proinflammatory cytokines and injury to the contralateral kidneys [36]. Indeed, evaluation of the renal sections in our study showed patchy mild injury in the contralateral sham-operated kidneys, possibly accounting for the lack of significant difference in the ^{13}C Lac/Pyr ratio or the tissue LDH activity between the sham-operated and IRI kidneys at day 7. Furthermore, renal LDH activity from a separate group of mice 7 days following sham operation without unilateral IRI was significantly lower than that of the IRI kidneys or the contralateral sham-operated kidneys in the unilateral IRI model. This suggests that the ^{13}C Lac/Pyr finding in our unilateral IRI model was not simply due to the effects of sham operation.

We also evaluated the ratio of ^{13}C Bic/Lac as a measure of the balance between oxidative pyruvate metabolism and glycolysis. We found that the ^{13}C Bic/Lac ratio in the IRI kidneys was approximately 51% lower at day 7 when compared to baseline, and the ^{13}C Bic/Lac ratio was significantly lower in the IRI kidneys when compared to that in the contralateral sham-operated kidneys at day 7. The Bic/Lac ratio has been suggested to serve as a sensitive metric for the opposing changes in the conversion of pyruvate to bicarbonate and lactate [37–39]. Additionally, as both bicarbonate and lactate are produced from pyruvate, the Bic/Lac ratio can be used to control for changes in perfusion between baseline and following IRI [40]. Although there was reduced perfusion in the IRI kidneys, the lower Bic/Lac ratio in the IRI kidneys at day 7 indicates that the lower ^{13}C bicarbonate production was not simply due to lower delivery of the ^{13}C pyruvate.

As has been previously reported [41], we found lower renal cortex perfusion in the kidneys subjected to IRI using ASL MRI. This technique has previously been used to quantify perfusion impairment in renal allografts in human and animal studies, in patients with renal artery stenosis, and in a murine model of unilateral IRI [41–43]. The perfusion values measured in the kidneys at baseline and following unilateral IRI in our study are in

agreement with those reported in the literature [41, 44]. The reduction in renal perfusion and persistent hypoxia likely contribute to the oxidative stress and mitochondrial dysfunction in the injured kidneys.

Recent studies have also reported the utilization of HP urea and HP water to image renal perfusion [45–49]. For example, in a rat model of IRI, Nielsen and colleagues showed a significant reduction in the HP ^{13}C, ^{15}N-urea distribution in the injured kidney which could be due to a combination of reduced blood flow and altered urea transport [45]. Ardenkjaer-Larsen and colleagues demonstrated in swine that renal cortical perfusion can be measured using high-contrast dynamic HP water imaging [48]. Future studies combining multiple HP probes to simultaneously assess perfusion and metabolism are warranted to further interrogate the multiple molecular events that occur during progressive kidney injuries.

Prior studies have demonstrated the key role oxidative stress plays in both AKI and the subsequent transition to CKD. For example, Basile et al. showed in a rat model of AKI that there was sustained renal oxidative stress following recovery from AKI that altered both renal hemodynamics and fibrotic responses, and may contribute to the transition from AKI to CKD [50]. Clinically, noninvasive monitoring of the redox capacity at such time points may provide a risk assessment of potential progression to CKD.

Accumulating evidence emphasizes the impact of mitochondrial dysfunction in the progression of tubular damage following AKI. For example, a recent study by Lan et al. showed that mitochondria were greatly reduced in number and of smaller size in renal tubules that progress to atrophy following IRI [12]. Importantly, they also showed that metabolic alterations played a key role in the development of renal tubule atrophy and transition to CKD. Specifically, tubules that have dysfunctional repair and progress to atrophy following AKI have increased phosphorylation of the mitochondrial enzyme PDH which decreases PDH activity [12]. In our study, we showed that the reduced activity of the mitochondrial PDH in the injured kidneys can be monitored by measuring the HP ^{13}C bicarbonate production. This could be a noninvasive strategy to assess the mitochondrial metabolic alteration associated with progressive renal injury.

Our finding of decreased HP ^{13}C bicarbonate production following IRI is in agreement with those from a recent study by Nielsen and colleagues which reported lower HP ^{13}C pyruvate conversion to bicarbonate in a rat model of unilateral IRI with 60 minutes of ischemia followed by 24 hour of reperfusion [51]. However, the investigators in that study also showed a decrease in ^{13}C pyruvate conversion to lactate in the kidneys subjected to IRI. In contrast, we found an increase in the ^{13}C Lac/Pyr ratio at day 7 in the IRI kidneys, although the ^{13}C Lac/Pyr ratio was not significantly different between the IRI kidneys and contralateral sham-operated kidneys at day 7. The discrepancy between the findings is likely attributable to the time of assessment. The study by Nielsen et al was performed at 24 hours following IRI when many renal tubules were likely necrotic, with attendant loss of cellular LDH and low pyruvate conversion to lactate [51]. Indeed, other murine studies have shown significantly depressed renal LDH levels 18–24 hours following IRI due to LDH release from necrotic cells [52, 53]. In contrast, our studies were performed 7 days following IRI, at which time we have shown that acute tubular necrosis was diminished with areas of tubular

epithelial cell regeneration. Our finding is in agreement with those from the study by Lan et al who reported that rat kidneys at 7 days following IRI showed evidence of dedifferentiation, regeneration, and increased glycolytic enzyme expression and lactate concentration [12]. This could explain our observation of the increase in the ^{13}C Lac/Pyr ratio in the IRI kidneys at day 7 when compared to baseline. Taken together, these data suggest the presence of dynamic changes in pyruvate metabolism over time following IRI, and future studies are warranted to evaluate the metabolic changes at multiple early and delayed time points following injury.

It is becoming increasingly clear that patients who survive an episode of AKI are at high risk of subsequent CKD and end-stage renal disease [4, 54]. Published studies have also indicated that more intensive monitoring of patients following an episode of AKI has the potential to identify early the evolution to CKD, and to mitigate complications associated with CKD [55–57]. Such studies highlight the unmet clinical need for additional metrics to identify patients at risk for developing CKD following AKI. Noninvasive approaches such as HP ^{13}C metabolic MR techniques potentially offer a way to risk stratify these patients. Additionally, there is increasing interest in developing drugs that target the molecular and metabolic events in progressive kidney injury. For example, Skrypnyk et al. have shown that pyridoxamine, a form of vitamin B6, interferes with oxidative macromolecular damage [13]. Pyridoxamine reduced both short- and long-term injury and fibrosis in a mouse model of IRI, and may prevent the transition of AKI to CKD [13]. Bendavia, a mitochondrial-targeted peptide has been shown to protect mitochondrial structure and function in an IRI model [14]. Therefore, the HP ^{13}C MR strategies described in our study could potentially provide mechanistically informative biomarkers to assess such targeted treatment effects *in vivo*.

Our study has several limitations. First, the HP ^{13}C MR acquisition was performed at a single time point after the injection of the substrates in order to maximize the signal of the metabolites, in particular the ^{13}C bicarbonate signal, in the mouse kidneys. The single time point acquisition could introduce variability in the data due to differences in perfusion and substrate delivery. Despite the lack of dynamic acquisition, we found significant differences in the metabolite ratios in the kidneys following injury. In future studies, improved substrate polarization, such as via the new 5T Spinlab DNP polarizer (GE Healthcare), may enable improved signal for dynamic acquisition. Second, we did not perform HP ^{13}C MR studies in a separate group of mice with sham operation without unilateral IRI. However, we showed that the renal LDH activity from mice 7 days following sham operation without unilateral IRI was lower than that of the IRI kidneys or the contralateral sham-operated kidneys in the unilateral IRI model. This suggests that the ^{13}C Lac/Pyr finding in our unilateral IRI model was not simply due to the effects of sham operation. Third, we performed HP ^{13}C DHA and ^{13}C pyruvate studies in two separate sessions in our study. Future studies utilizing co-polarization techniques [58] are warranted which will reduce the burden for the animals in pre-clinical studies and facilitate clinical translation of this technique. Forth, the spatial resolution of the HP MRS in this study is relatively coarse in relation to the small size of the mouse kidneys in this pre-clinical study. For example, the kidney structures most susceptible to IRI include the proximal renal tubules and medullary thick ascending limb, which are located in the kidney cortex and outer medulla [59]. However, the relatively large HP voxel likely also included parts of inner medulla of the kidney. Therefore the partial volume effect

would introduce variability in the measured HP metabolic data. Nonetheless, we found significant differences in several HP metabolite ratios following IRI. Potential ways to improve the spatial resolution of HP MRS include better substrate polarization, improved coil designs, and more efficient sampling of k-space. These advances will allow specific interrogation of the various renal compartments in pre-clinical models, as well as in future clinical studies in patients with kidney disease.

Notably, the safety and feasibility of HP ^{13}C pyruvate MR have already been demonstrated in the phase I clinical trial of HP ^{13}C pyruvate in prostate cancer patients [60], and more recently in human hearts [61]. While DHA is also an endogenous compound, intravenous administration of DHA has been reported to cause transient respiratory depression in a dose-dependent manner [20], and to cause elevation of blood pressure and salivation when injected at high dose in un-buffered solutions [62]. However other prior studies have reported no significant adverse effects when DHA dissolved in sodium acetate/sodium bicarbonate buffered solution was injected at high dose in rat models of cerebral ischemia and liver ischemia, and that DHA provided protection in these experimental model of ischemia reperfusion [63, 64]. A separate prior study reported that DHA had a diabetogenic effect in rats [65]; however subsequent studies suggested that the impurities in the DHA preparation as a cause for the reported diabetogenic effect [66], and that DHA protects against dioxin-induced toxicity in pancreatic beta cells [67]. The metabolic effects of the injected dose and the safety of ^{13}C DHA in humans will need to be established.

In summary, we have shown that HP ^{13}C metabolic MR can be used to noninvasively assess the altered renal redox capacity and mitochondrial PDH activity following ischemic reperfusion injury. Such an imaging approach can potentially enhance the prediction and monitoring of progressive kidney injury, as well as providing companion biomarkers that can better inform on the response to targeted therapies.

Acknowledgments

Grant Support: The work was supported by NIH R01DK097357 (ZJW), NIH R01CA166766 (DMW), NIH P41EB013598 (JK), Department of Veterans Affairs Merit Review Award I-1BX000593 (DHL), NIH RO1DK39776 (DHL), and the resources and facilities at the San Francisco VA Medical Center.

Abbreviations

HP	hyperpolarized
IRI	ischemia reperfusion injury
AKI	acute kidney injury
CKD	chronic kidney disease
PDH	pyruvate dehydrogenase
LDH	lactate dehydrogenase
ROS	reactive oxygen species

References

1. Venkatachalam MA, Griffin KA, Lan R, Geng H, Saikumar P, Bidani AK. Acute kidney injury: a springboard for progression in chronic kidney disease. American journal of physiology Renal physiology. 2010; 298(5):F1078–1094. [PubMed: 20200097]
2. Hsu CY. Yes, AKI truly leads to CKD. Journal of the American Society of Nephrology : JASN. 2012; 23(6):967–969. [PubMed: 22499588]
3. Bucaloiu ID, Kirchner HL, Norfolk ER, Hartle JE 2nd, Perkins RM. Increased risk of death and de novo chronic kidney disease following reversible acute kidney injury. Kidney international. 2012; 81(5):477–485. [PubMed: 22157656]
4. Coca SG, Singanamala S, Parikh CR. Chronic kidney disease after acute kidney injury: a systematic review and meta-analysis. Kidney international. 2012; 81(5):442–448. [PubMed: 22113526]
5. Hoerger TJ, Simpson SA, Yarnoff BO, Pavkov ME, Rios Burrows N, Saydah SH, Williams DE, Zhuo X. The future burden of CKD in the United States: a simulation model for the CDC CKD Initiative. American journal of kidney diseases : the official journal of the National Kidney Foundation. 2015; 65(3):403–411. [PubMed: 25468386]
6. Okamura DM, Himmelfarb J. Tipping the redox balance of oxidative stress in fibrogenic pathways in chronic kidney disease. Pediatric nephrology. 2009; 24(12):2309–2319. [PubMed: 19421784]
7. Okamura DM, Pennathur S. The balance of powers: Redox regulation of fibrogenic pathways in kidney injury. Redox biology. 2015; 6:495–504. [PubMed: 26448394]
8. Takasu O, Gaut JP, Watanabe E, To K, Fagley RE, Sato B, Jarman S, Efimov IR, Janks DL, Srivastava A, et al. Mechanisms of cardiac and renal dysfunction in patients dying of sepsis. American journal of respiratory and critical care medicine. 2013; 187(5):509–517. [PubMed: 23348975]
9. Parekh DJ, Weinberg JM, Ercole B, Torkko KC, Hilton W, Bennett M, Devarajan P, Venkatachalam MA. Tolerance of the human kidney to isolated controlled ischemia. Journal of the American Society of Nephrology : JASN. 2013; 24(3):506–517. [PubMed: 23411786]
10. Ishimoto Y, Inagi R. Mitochondria: a therapeutic target in acute kidney injury. Nephrology, dialysis, transplantation : official publication of the European Dialysis and Transplant Association - European Renal Association. 2016; 31(7):1062–1069.
11. Tran M, Tam D, Bardia A, Bhasin M, Rowe GC, Kher A, Zsengeller ZK, Akhavan-Sharif MR, Khankin EV, Saintgeniez M, et al. PGC-1alpha promotes recovery after acute kidney injury during systemic inflammation in mice. The Journal of clinical investigation. 2011; 121(10):4003–4014. [PubMed: 21881206]
12. Lan R, Geng H, Singha PK, Saikumar P, Bottinger EP, Weinberg JM, Venkatachalam MA. Mitochondrial Pathology and Glycolytic Shift during Proximal Tubule Atrophy after Ischemic AKI. Journal of the American Society of Nephrology : JASN. 2016
13. Skrypnyk NI, Voziyan P, Yang H, de Caestecker CR, Theberge MC, Drouin M, Hudson B, Harris RC, de Caestecker MP. Pyridoxamine reduces postinjury fibrosis and improves functional recovery after acute kidney injury. American journal of physiology Renal physiology. 2016; 311(2):F268–277. [PubMed: 27194713]
14. Birk AV, Liu S, Soong Y, Mills W, Singh P, Warren JD, Seshan SV, Pardee JD, Szeto HH. The mitochondrial-targeted compound SS-31 re-energizes ischemic mitochondria by interacting with cardiolipin. Journal of the American Society of Nephrology : JASN. 2013; 24(8):1250–1261. [PubMed: 23813215]
15. Golman K, in 't Zandt R, Thaning M. Real-time metabolic imaging. Proc Natl Acad Sci U S A. 2006; 103(30):11270–11275. [PubMed: 16837573]
16. Kurhanewicz J, Bok R, Nelson SJ, Vigneron DB. Current and potential applications of clinical 13C MR spectroscopy. Journal of nuclear medicine : official publication, Society of Nuclear Medicine. 2008; 49(3):341–344.
17. Ardenkjaer-Larsen JH, Fridlund B, Gram A, Hansson G, Hansson L, Lerche MH, Servin R, Thaning M, Golman K. Increase in signal-to-noise ratio of > 10,000 times in liquid-state NMR. Proc Natl Acad Sci U S A. 2003; 100(18):10158–10163. [PubMed: 12930897]

18. Keshari KR, Wilson DM, Sai V, Bok R, Jen KY, Larson P, Van Criekinge M, Kurhanewicz J, Wang ZJ. Noninvasive in vivo imaging of diabetes-induced renal oxidative stress and response to therapy using hyperpolarized 13C dehydroascorbate magnetic resonance. Diabetes. 2015; 64(2):344–352. [PubMed: 25187363]

19. Keshari KR, Sai V, Wang ZJ, Vanbrocklin HF, Kurhanewicz J, Wilson DM. Hyperpolarized [1–13C]dehydroascorbate MR spectroscopy in a murine model of prostate cancer: comparison with 18F-FDG PET. Journal of nuclear medicine : official publication, Society of Nuclear Medicine. 2013; 54(6):922–928.

20. Timm KN, Hu DE, Williams M, Wright AJ, Kettunen MI, Kennedy BW, Larkin TJ, Dzien P, Marco-Rius I, Bohndiek SE, et al. Assessing oxidative stress in tumors by measuring the rate of hyperpolarized [1–13C]dehydroascorbic acid reduction using 13C magnetic resonance spectroscopy. The Journal of biological chemistry. 2016

21. Atherton HJ, Schroeder MA, Dodd MS, Heather LC, Carter EE, Cochlin LE, Nagel S, Sibson NR, Radda GK, Clarke K, et al. Validation of the in vivo assessment of pyruvate dehydrogenase activity using hyperpolarised 13C MRS. NMR in biomedicine. 2011; 24(2):201–208. [PubMed: 20799252]

22. Schroeder MA, Atherton HJ, Heather LC, Griffin JL, Clarke K, Radda GK, Tyler DJ. Determining the in vivo regulation of cardiac pyruvate dehydrogenase based on label flux from hyperpolarised [1–13C]pyruvate. NMR in biomedicine. 2011; 24(8):980–987. [PubMed: 21387444]

23. Wan X, Hou L, Zhang L, Huang W, Liu L, Zhang Q, Hu B, Chen W, Chen X, Cao C. IKKa is involved in kidney recovery and regeneration of acute ischemia/reperfusion injury in mmice through IL10-producing regulatory T cells. Disease Models & Mechanisms. 2015:733–742. [PubMed: 26035380]

24. Keshari KR, Kurhanewicz J, Bok R, Larson PE, Vigneron DB, Wilson DM. Hyperpolarized 13C dehydroascorbate as an endogenous redox sensor for in vivo metabolic imaging. Proc Natl Acad Sci U S A. 2011; 108(46):18606–18611. [PubMed: 22042839]

25. Liang WJ, Johnson D, Jarvis SM. Vitamin C transport systems of mammalian cells. Molecular membrane biology. 2001; 18(1):87–95. [PubMed: 11396616]

26. Cunningham CH, Chen AP, Albers MJ, Kurhanewicz J, Hurd RE, Yen YF, Pauly JM, Nelson SJ, Vigneron DB. Double spin-echo sequence for rapid spectroscopic imaging of hyperpolarized 13C. Journal of magnetic resonance. 2007; 187(2):357–362. [PubMed: 17562376]

27. Crane JC, Olson MP, Nelson SJ. SIVIC: Open-Source, Standards-Based Software for DICOM MR Spectroscopy Workflows. International journal of biomedical imaging. 2013; 2013:169526. [PubMed: 23970895]

28. Von Morze C, Chang GY, Larson PE, Shang H, Allu PK, Bok R, Crane JC, Olson MP, Tan CT, Marco-Rius I, et al. Detection of localized changes in the metabolism of hyperpolarized gluconeogenic precursors 13C-lactate and 13C-pyruvate in kidney and liver. Magnetic resonance in medicine. 2016 [Epub ahead of print].

29. Prevost VH, Girard OM, Callot V, Cozzone Pr PJ, Duhamel G. Fast imaging strategies for mouse kidney perfusion measurement with pseudocontinuous arterial spin labeling (pCASL) at ultra high magnetic field (11.75 tesla). Journal of magnetic resonance imaging : JMRI. 2015; 42(4):999–1008. [PubMed: 25712197]

30. Pell GS, Thomas DL, Lythgoe MF, Calamante F, Howseman AM, Gadian DG, Ordidge RJ. Implementation of quantitative FAIR perfusion imaging with a short repetition time in time-course studies. Magnetic resonance in medicine. 1999; 41(4):829–840. [PubMed: 10332861]

31. Cheong B, Muthupillai R, Rubin MF, Flamm SD. Normal values for renal length and volume as measured by magnetic resonance imaging. Clinical journal of the American Society of Nephrology : CJASN. 2007; 2(1):38–45. [PubMed: 17699385]

32. Day YJ, Huang L, Ye H, Li L, Linden J, Okusa MD. Renal ischemia-reperfusion injury and adenosine 2A receptor-mediated tissue protection: the role of CD4+ T cells and IFN-gamma. Journal of immunology. 2006; 176(5):3108–3114.

33. Wells WW, Xu DP, Yang YF, Rocque PA. Mammalian thioltransferase (glutaredoxin) and protein disulfide isomerase have dehydroascorbate reductase activity. The Journal of biological chemistry. 1990; 265(26):15361–15364. [PubMed: 2394726]

34. Whitbread AK, Masoumi A, Tetlow N, Schmuck E, Coggan M, Board PG. Characterization of the omega class of glutathione transferases. Methods in enzymology. 2005; 401:78–99. [PubMed: 16399380]
35. Weinberg JM, Molitoris BA. Illuminating mitochondrial function and dysfunction using multiphoton technology. Journal of the American Society of Nephrology : JASN. 2009; 20(6): 1164–1166. [PubMed: 19470668]
36. Meldrum KK, Meldrum DR, Meng X, Ao L, Harken AH. TNF-alpha-dependent bilateral renal injury is induced by unilateral renal ischemia-reperfusion. American journal of physiology Heart and circulatory physiology. 2002; 282(2):H540–546. [PubMed: 11788401]
37. Merritt ME, Harrison C, Storey C, Sherry AD, Malloy CR. Inhibition of carbohydrate oxidation during the first minute of reperfusion after brief ischemia: NMR detection of hyperpolarized 13CO2 and H13CO3. Magnetic resonance in medicine. 2008; 60(5):1029–1036. [PubMed: 18956454]
38. Ball DR, Cruickshank R, Carr CA, Stuckey DJ, Lee P, Clarke K, Tyler DJ. Metabolic imaging of acute and chronic infarction in the perfused rat heart using hyperpolarised [1–13C]pyruvate. NMR in biomedicine. 2013; 26(11):1441–1450. [PubMed: 23775685]
39. Park JM, Spielman D, Josan S, Jang T, Merchant M, Hurd R, Mayer D, Recht LD. Hyperpolarized (13)C-lactate to (13)C-bicarbonate ratio is a biomakerr for monitoring the acute response of anti-vascular endothelial growth factor (anti-VEGF) treatment. NMR in biomedicine. 2016; 29(5):650–659. [PubMed: 26990457]
40. Yoshihara HA, Bastiaansen JA, Berthonneche C, Comment A, Schwitter J. An intact small animal model of myocardial ischemia-reperfusion: Characterization of metabolic changes by hyperpolarized 13C MR spectroscopy. American journal of physiology Heart and circulatory physiology. 2015; 309(12):H2058–2066. [PubMed: 26453328]
41. Hueper K, Gutberlet M, Rong S, Hartung D, Mengel M, Lu X, Haller H, Wacker F, Meier M, Gueler F. Acute kidney injury: arterial spin labeling to monitor renal perfusion impairment in mice-comparison with histopathologic results and renal function. Radiology. 2014; 270(1):117–124. [PubMed: 24023073]
42. Heusch P, Wittsack HJ, Blondin D, Ljimani A, Nguyen-Quang M, Martirosian P, Zenginli H, Bilk P, Kropil P, Heusner TA, et al. Functional evaluation of transplanted kidneys using arterial spin labeling MRI. Journal of magnetic resonance imaging : JMRI. 2014; 40(1):84–89. [PubMed: 24123319]
43. Ebrahimi B, Crane JA, Knudsen BE, Macura SI, Grande JP, Lerman LO. Evolution of cardiac and renal impairment detected by high-field cardiovascular magnetic resonance in mice with renal artery stenosis. Journal of cardiovascular magnetic resonance : official journal of the Society for Cardiovascular Magnetic Resonance. 2013; 15:98. [PubMed: 24160179]
44. Duhamel G, Prevost V, Girard OM, Callot V, Cozzone PJ. High-resolution mouse kidney perfusion imaging by pseudo-continuous arterial spin labeling at 11.75T. Magn Reson Med. 2014; 71(3): 1186–1196. [PubMed: 23568817]
45. Nielsen PM, Szocska Hansen ES, Norlinger TS, Norregaard R, Bonde Bertelsen L, Stodkilde Jorgensen H, Laustsen C. Renal ischemia and reperfusion assessment with three-dimensional hyperpolarized 13 C,15 N2-urea. Magnetic resonance in medicine. 2016; 76(5):1524–1530. [PubMed: 27548739]
46. Bertelsen LB, Nielsen PM, Qi H, Norlinger TS, Zhang X, Stodkilde-Jorgensen H, Laustsen C. Diabetes induced renal urea transport alterations assessed with 3D hyperpolarized 13 C,15 N-Urea. Magnetic resonance in medicine. 2016
47. Ardenkjaer-Larsen JH, Laustsen C, Bowen S, Rizi R. Hyperpolarized H2 O MR angiography. Magnetic resonance in medicine. 2014; 71(1):50–56. [PubMed: 24243653]
48. Wigh Lipso K, Hansen ES, Tougaard RS, Laustsen C, Ardenkjaer-Larsen JH. Renal MR angiography and perfusion in the pig using hyperpolarized water. Magnetic resonance in medicine. 2016
49. von Morze C, Bok RA, Reed GD, Ardenkjaer-Larsen JH, Kurhanewicz J, Vigneron DB. Simultaneous multiagent hyperpolarized (13)C perfusion imaging. Magnetic resonance in medicine. 2014; 72(6):1599–1609. [PubMed: 24382698]

50. Basile DP, Leonard EC, Beal AG, Schleuter D, Friedrich J. Persistent oxidative stress following renal ischemia-reperfusion injury increases ANG II hemodynamic and fibrotic activity. American journal of physiology Renal physiology. 2012; 302(11):F1494–1502. [PubMed: 22442209]
51. Nielsen PM, Laustsen C, Bertelsen LB, Qiu H, Mikkelsen E, Kristensen ML, Norregaard R, Stodkilde-Jorgensen H. In situ lactate dehydrogenase activity-a novel renal cortical imaging biomarker of tubular injury? American journal of physiology Renal physiology. 2016 Epub ahead of print.
52. Zager RA, Johnson AC, Becker K. Renal Cortical Lactate Dehydrogenase: A Useful, Accurate, Quantitative Marker of In Vivo Tubular Injury and Acute Renal Failure. PloS one. 2013; 8(6):e66776. [PubMed: 23825563]
53. Zager RA, Johnson AC, Becker K. Renal cortical pyruvate depletion during AKI. Journal of the American Society of Nephrology : JASN. 2014; 25(5):998–1012. [PubMed: 24385590]
54. Chawla LS, Amdur RL, Shaw AD, Faselis C, Palant CE, Kimmel PL. Association between AKI and long-term renal and cardiovascular outcomes in United States veterans. Clinical journal of the American Society of Nephrology : CJASN. 2014; 9(3):448–456. [PubMed: 24311708]
55. Goldstein SL, Jaber BL, Faubel S, Chawla LS, Acute Kidney Injury Advisory Group of American Society of N. AKI transition of care: a potential opportunity to detect and prevent CKD. Clinical journal of the American Society of Nephrology : CJASN. 2013; 8(3):476–483. [PubMed: 23471414]
56. Chawla LS, Eggers PW, Star RA, Kimmel PL. Acute kidney injury and chronic kidney disease as interconnected syndromes. The New England journal of medicine. 2014; 371(1):58–66. [PubMed: 24988558]
57. Smart NA, Titus TT. Outcomes of early versus late nephrology referral in chronic kidney disease: a systematic review. The American journal of medicine. 2011; 124(11):1073–1080 e1072. [PubMed: 22017785]
58. Wilson DM, Keshari KR, Larson PE, Chen AP, Hu S, Van Criekinge M, Bok R, Nelson SJ, Macdonald JM, Vigneron DB, et al. Multi-compound polarization by DNP allows simultaneous assessment of multiple enzymatic activities in vivo. Journal of magnetic resonance. 2010; 205(1): 141–147. [PubMed: 20478721]
59. Eckardt KU, Bernhardt WM, Weidemann A, Warnecke C, Rosenberger C, Wiesener MS, Willam C. Role of hypoxia in the pathogenesis of renal disease. Kidney international Supplement. 2005; (99):S46–51.
60. Nelson SJ, Kurhanewicz J, Vigneron DB, Larson PE, Harzstark AL, Ferrone M, van Criekinge M, Chang JW, Bok R, Park I, et al. Metabolic Imaging of Patients with Prostate Cancer Using Hyperpolarized [1–13C]Pyruvate. Science translational medicine. 2013; 5(198):198ra108.
61. Cunningham CH, Lau JY, Chen AP, Geraghty BJ, Perks WJ, Roifman I, Wright GA, Connelly KA. Hyperpolarized 13C Metabolic MRI of the Human Heart: Initial Experience. Circulation research. 2016
62. Patterson JW, Mastin DW. Some effects of dehydroascorbic acid on the central nervous system. The American journal of physiology. 1951; 167(1):119–126. [PubMed: 14885478]
63. Huang J, Agus DB, Winfree CJ, Kiss S, Mack WJ, McTaggart RA, Choudhri TF, Kim LJ, Mocco J, Pinsky DJ, et al. Dehydroascorbic acid, a blood-brain barrier transportable form of vitamin C, mediates potent cerebroprotection in experimental stroke. Proc Natl Acad Sci U S A. 2001; 98(20):11720–11724. [PubMed: 11573006]
64. De Tata V, Brizzi S, Saviozzi M, Lazzarotti A, Fierabracci V, Malvaldi G, Casini A. Protective role of dehydroascorbate in rat liver ischemia-reperfusion injury. The Journal of surgical research. 2005; 123(2):215–221. [PubMed: 15680381]
65. Patterson JW. Diabetogenic effect of dehydroglucoascorbic acid. Science. 1950; 111(2896):724–725. [PubMed: 15431071]
66. Domke I, Weis W. Reinvestigation of the diabetogenic effect of dehydroascorbic acid. International journal for vitamin and nutrition research Internationale Zeitschrift fur Vitamin- und Ernahrungsforschung Journal international de vitaminologie et de nutrition. 1983; 53(1):51–60. [PubMed: 6853059]

67. Martino L, Novelli M, Masini M, Chimenti D, Piaggi S, Masiello P, De Tata V. Dehydroascorbate protection against dioxin-induced toxicity in the beta-cell line INS-1E. Toxicology letters. 2009; 189(1):27–34. [PubMed: 19414064]

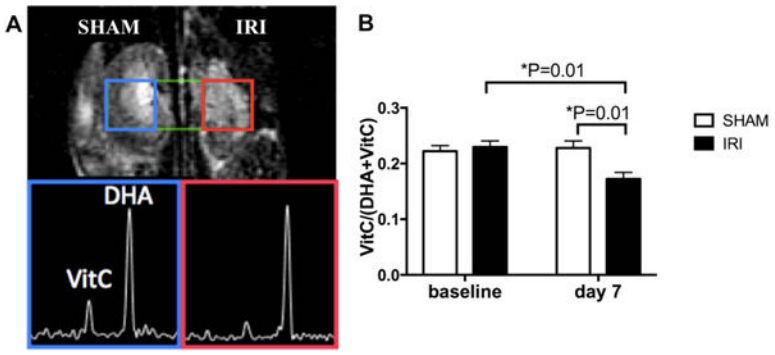

Fig.1.

A: Representative voxel placement and HP DHA ^{13}C spectra in the kidney subjected to IRI and the contralateral sham-operated kidney at day 7. **B**: HP ^{13}C VitC/(VitC+DHA) ratio at baseline and day 7. The kidneys subjected to IRI showed significantly lower VitC/(VitC +DHA) ratio at day 7 when compared to baseline, and when compared to the contralateral sham-operated kidneys at day 7.

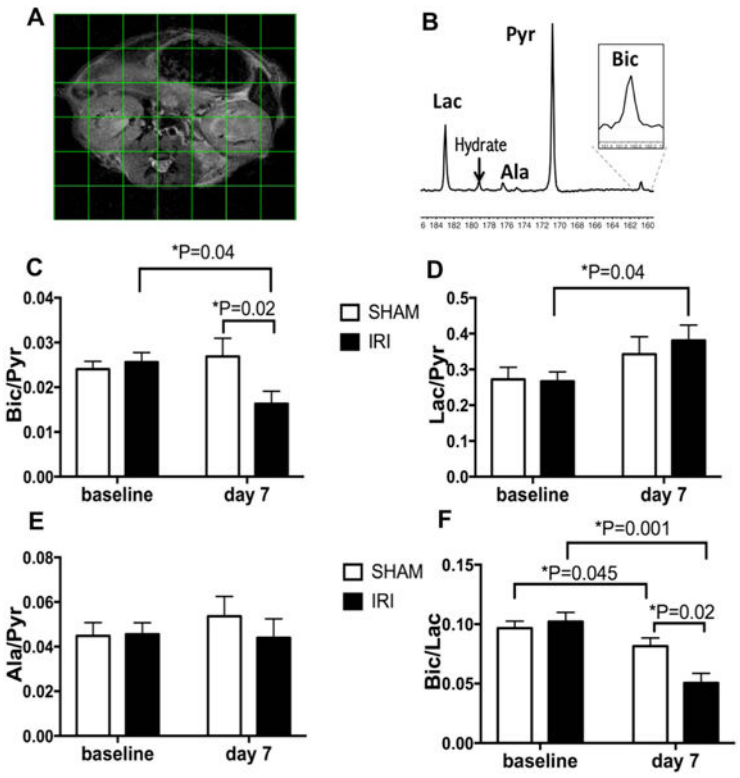

Fig. 2.

A: Overlay of the voxel placement from the 2D chemical shift acquisition on the T2 weighted anatomic image. **B**: Representative spectrum through the kidney voxel after the injection of HP ^{13}C pyruvate in the IRI kidney at day 7. HP ^{13}C metabolites visualized included lactate (Lac), alanine (Ala), and bicarbonate (Bic). Hydrate=^{13}C pyruvate hydrate. **C**: The kidneys subjected to IRI showed significantly lower ^{13}C Bic/Pyr ratio at day 7 when compared to the baseline, and when compared to the contralateral sham-operated kidneys at day 7. **D**: The HP ^{13}C Lac/Pyr ratio increased significantly from baseline to day 7 in the IRI kidneys. However, the ^{13}C Lac/Pyr ratio was not significantly different between the IRI and the contralateral sham-operated kidneys at day 7. **E**: The HP ^{13}C Ala/Pyr ratio remained the same following IRI. **F**: The HP ^{13}C Bic/Lac ratio decreased significantly from baseline to day 7 in the IRI kidneys. The ^{13}C Bic/Lac ratio also decreased slightly from baseline to day 7 in the contralateral sham-operated kidneys. The ^{13}C Bic/Lac ratio was significantly lower in the IRI than the contralateral sham-operated kidneys at day 7.

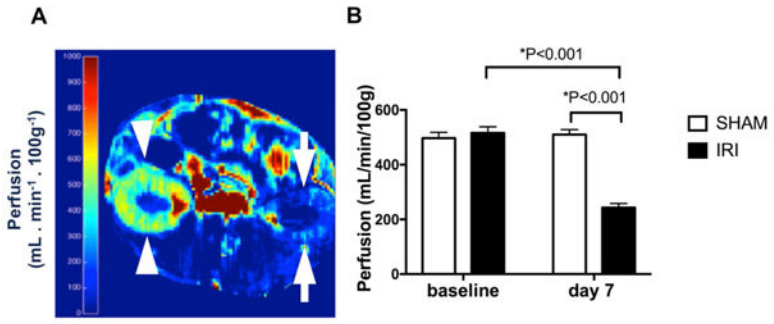

Fig. 3.

A: Example of a renal perfusion map as measured by ^{1}H ASL MRI (Kidney subjected to IRI: arrows; contralateral sham-operated kidney: arrowheads). **B**: The kidneys subjected to IRI showed a significant decrease in perfusion, while the perfusion remained virtually unchanged in the contralateral sham-operated kidneys.

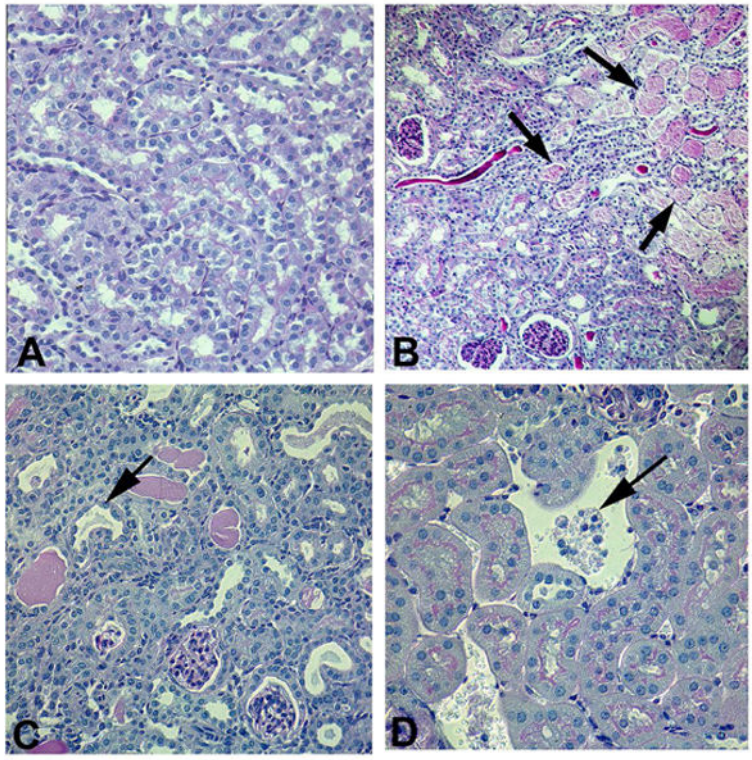

Fig. 4.

Histologic features of unilateral IRI model on PAS stained renal sections. **A**: Kidneys from control mice not subjected to IRI showed normal tubular structures. **B**: Kidneys at 48 hours after being subjected to unilateral IRI showed moderate injury with tubular dilatation and cast formation (arrows). **C**: Kidneys at 7 days after being subjected to unilateral IRI showed decreased tubular dilatation and cast formation, associated with regenerating tubular epithelial cells (arrow). **D**: The contralateral sham-operated kidneys at day 7 showed scattered foci of tubular epithelial cell necrosis associated with cellular cast formation (arrow). A, B, C: × 200 magnification. D: × 400 magnification.

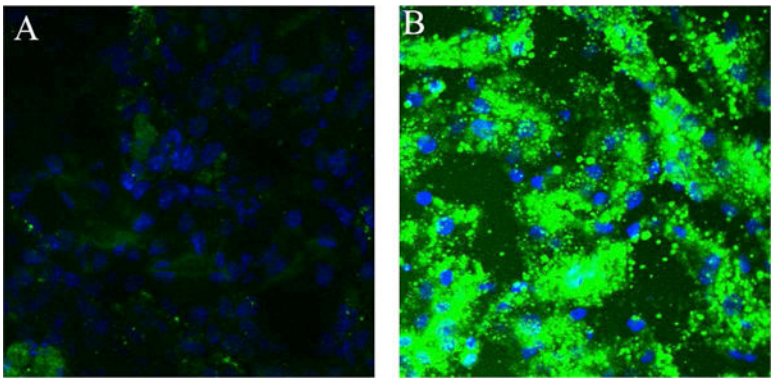

Fig. 5.

Example of DCF staining of the renal sections. The kidneys subjected to IRI (**B**) showed markedly higher DCF staining (green color) consistent with increased level of reactive oxygen species (ROS), when compared to the contralateral sham-operated kidneys (**A**) at day 7.

Table 1

Body weight, blood urea nitrogen level, and kidney volume as measured by MRI at baseline and 7 days following unilateral IRI.

	Body weight (g)	BUN (mg/dL)	Kidney volume (mm^3)	
			Sham-operated	IRI
Baseline	29.7±0.7	25.5±1.2	0.26±0.01	0.24±0.01
Day 7	28.5±0.9	36.4±2.0[a]	0.32±0.01[b]	0.24±0.01

Data are mean±SE.

[a] $p < 0.005$ baseline vs. day 7;

[b] $p<0.0005$ baseline vs. day7 for the sham-operated kidneys. BUN: blood urea nitrogen. IRI: ischemia reperfusion injury.